Coral Reefs (2004) 23: 109–122
DOI 10.1007/s00338-003-0352-z

REPORT

S. Ouillon · P. Douillet · S. Andréfouët

Coupling satellite data with in situ measurements and numerical modeling to study fine suspended-sediment transport: a study for the lagoon of New Caledonia

Received: 12 March 2003 / Accepted: 20 May 2003 / Published online: 28 November 2003

Abstract This paper investigates the potential of remotely sensed data to map turbidity in a coral reef lagoon and to calibrate a numerical model of fine suspended-sediment transport. Simultaneous measurements of turbidity depth-profile and above-water spectral reflectance integrated according Landsat 7 ETM+ band 2 spectral sensitivity provide a linear regression relationship for the southwest lagoon of New Caledonia ($r^2 = 0.95$, $n = 40$). This relationship is applied to an empirically atmospherically corrected Landsat ETM+ image of the lagoon acquired on October 23, 2002. A comparison between Landsat estimates of turbidity and concurrent measurements at 14 stations indicates that the mean standard error in the satellite-estimated turbidity is 17.5%. The numerical model introduced in Douillet et al. (2001) is used to simulate the transport of fine suspended sediments in the lagoon in October 2002. A calibration of the erosion rate coefficient required by the model is proposed using in situ turbidity profiles and the remotely sensed turbidity field. In situ data are used to tune locally the erosion rate coefficient, while satellite data are used to determine its spatial zonation. We discuss necessary improvements in coupled studies of fine-sediment transport in coastal zones, namely relationships between turbidity and sediment concentration, integration of wave influence in the model, and correction of bottom reflection in satellite data processing.

Keywords Sediment transport · Suspended matter · Numerical model · Remote sensing · Ocean color · Erosion · New Caledonia · Lagoon · Landsat

S. Ouillon (✉) · P. Douillet
UR Camélia, IRD, BP A5, 98848 Nouméa, New Caledonia
E-mail: sylvain.ouillon@noumea.ird.nc
Tel.: +687-26-0729
Fax: +687-26-4326

S. Ouillon
LSEET/CNRS, Université de Toulon et du Var,
BP 132, 83957 La Garde cedex, France

S. Andréfouët
College of Marine Science,
Institute for Marine Remote Sensing,
University of South Florida,
140 7th Av. South, St Petersburg, FL 33701, USA

S. Andréfouët
UR Coréus, IRD, BP A5, 98848 Nouméa, New Caledonia

Introduction

Suspended matter plays an important role in water quality management because it is related to total primary production (transport of nutrients, reduction of light penetration) and to fluxes of metals, radio-nuclides and organic micropollutants. Its fluxes and dynamics are of primary importance to the biochemical functioning of coral reef ecosystems. Changes in sediment supplies and concentrations, and consequently changes in light penetration, may have significant consequences on coral health (e.g. Hudson 1981; Done 1982; Kleypas et al. 1999; Woolfe and Larcombe 1999; Alibert et al. 2003). Because developing open cast mining plays a significant and increasing economic role in New Caledonia, since 1996 a scientific program has been devoted to the study of anthropogenic and terrigenous effects on the 2,000 km^2 southwest lagoon around Nouméa where about half of the island population lives (see Fig. 1). Based on a long-term study of the lagoon sedimentology (Debenay 1987; Chardy et al. 1988; Clavier et al. 1995) and hydrodynamics (Jarrige et al. 1975; Morlière and Crémoux 1981; Douillet 1998), a three-dimensional model for the transport into suspension of mud particles has been recently developed (Douillet et al. 2001). Once fully calibrated and validated, this model will be used to estimate particle budget and sedimentary fluxes to follow the dynamics of river plumes and dredging releases, which will be coupled with a biological model of the lagoon. The model is calibrated and validated by recurrent cruises that provide only few points on different areas of the lagoon. Here, we investigate the

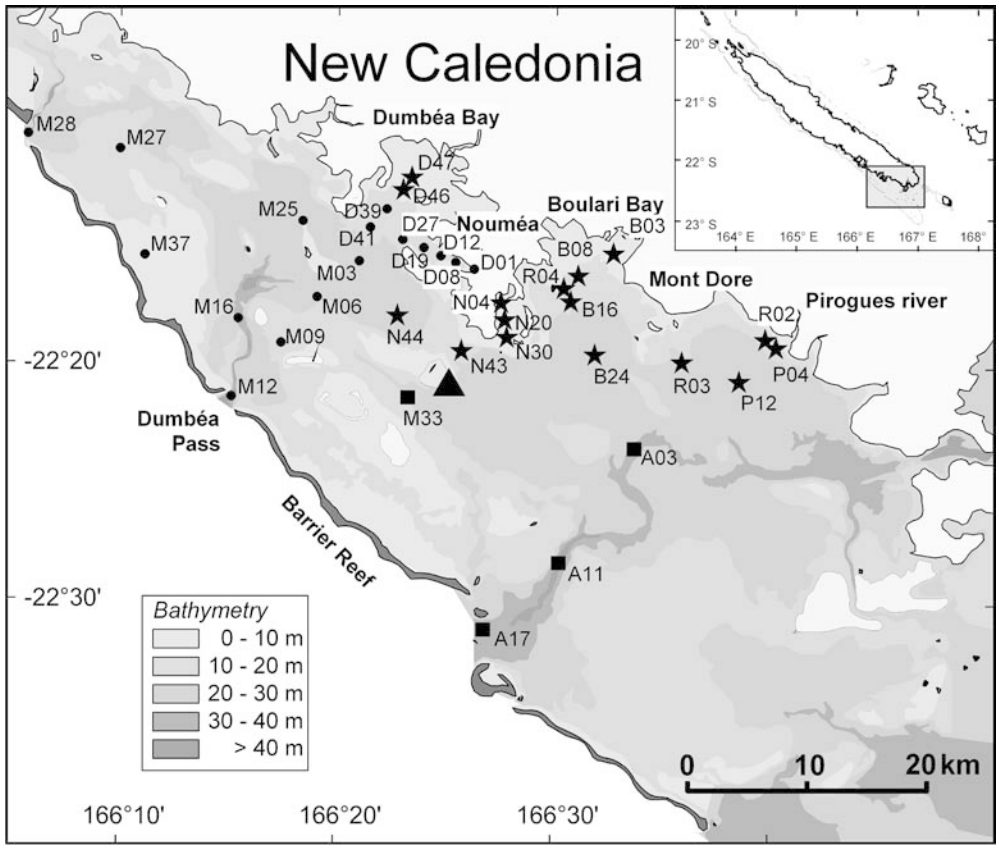

Fig. 1 The southwest lagoon of New Caledonia (SLNC). Location of meteorological station (▲), optical stations on October 23, 2002 making up population 2 (★), optical stations on October 22, 2002 included in population 1 (●), and supplementary turbidity profiles on October 23, 2002 (■)

possibility of using synoptic remotely sensed data to perform similar tasks.

Visible remote sensing can be used to map the distribution of surface turbidity or suspended particulate matter (SPM) concentrations (e.g. Ritchie et al. 1990; You and Hou 1992; Forget and Ouillon 1998; Doxaran et al. 2002). For the last 10 years, protocols for optical measurements at sea have been improved (Mobley 1999; Fargion and Mueller 2000). Recent studies focusing on different aspects of the sediment influence on the upwelling sea radiance (Lee et al. 2001; Mikkelsen 2002; Ouillon 2003) and the use of neural networks (e.g. Keiner and Yan 1998; Schiller and Doerffer 1999) have improved inversion methods. As a consequence of these recent developments, in situ and remotely sensed optical data contribute to the quantification of SPM concentrations in coastal waters with an uncertainty of less than 30%.

Measuring SPM by satellite at a given time is only one aspect of the problem. Understanding the dynamics of sedimentation warrants further development, including use of numerical models of circulation and sediment transport. In that context, remote sensing may also be helpful in the calibration and validation of such models. Early integrated studies compared SPM spatial patterns between satellite data and numerical simulations (e.g. Ouillon and Caussade 1991; Puls et al. 1994; Estournel et al. 1997). At that time, the lack of in situ data and the uncertainty in the inversion procedure limited the use of satellite data to describe spatial patterns and relative variations of SPM concentrations rather than their absolute values (e.g. Baban 1995, using the Landsat Thematic Mapper). The most recent integrated studies focus on river plumes (Jorgensen and Edelvang 2000; Durand et al. 2002) and lakes (Booth et al. 2000). Attempts to quantitatively compare SPM fields from images and models have been performed (Jorgensen and Edelvang 2000; Durand et al. 2002), but uncertainty on a number of parameters involved in the SPM transport model prevents their generalization. Remote sensing can be a valuable tool for estimating some of these physical parameters or thresholds. For example, using the Advanced Very High Resolution Radiometer (AVHRR) sensor and a numerical wave model, Booth et al. (2000) identified the thresholds of wind stress and direction that induce resuspension, as revealed by increasing reflectances.

Here we present an integrated study of suspended sediment transport in a coral reef lagoon involving field data, remote sensing, and numerical modeling. Landsat 7 Enhanced Thematic Mapper Plus (ETM+) data are combined with time-series of in situ optical and turbidity measurements to provide a turbidity field within the lagoon. The resulting map together with concurrent in situ measurements of vertical turbidity profiles are used to tune a key parameter of a SPM transport model. The model of fine suspended (silt and clay) particle transport we implemented is detailed in Douillet et al. (2001). This previous study evaluated the bulk critical shear stress

below which deposition (or above which erosion) occurs. Here, a refined parameterization of the erosion rate of particles is proposed to fit the model output with the turbidity field estimated from Landsat7 ETM + data acquired on October 23, 2002.

Methods

Study area

The lagoons of New Caledonia, located 1,500 km east of Australia, cover a total area of 23,400 km^2. The southwest lagoon of New Caledonia (denoted hereafter SLNC), around Nouméa, has a mean depth of approximately 17.5 m (Fig. 1). Two major factors control circulation in the SLNC: tide and wind (Douillet 1998). The most frequently encountered wind regime is the southeasterly trade wind (average speed 8 m s^{-1}, direction 110°, more than 2/3 of yearly wind occurrence). A description of the resulting current regime is given in Douillet et al (2001). Swell penetration into the lagoon is negligible, and wind-wave growth is limited by a fetch of a few tens of kilometers, providing mean wave length of less than 20 m and of less than 4-s period. However, the wave effects on resuspension in the shallower parts of the lagoon are likely significant. Three major lagoonal soft bottom benthic communities can be distinguished: muddy, grey-sand, and white-sand bottoms (Chardy et al. 1988). Terrigenous particles are almost absent from the sandy fraction except in the nearshore areas. Non-carbonated material (terrigenous and siliclastic) may reach 10% of the mud near the barrier reef and up to 80% in the bays (Clavier et al. 1995).

Field measurements

From June 2002 until January 2003, regular cruises provided the distribution of physical, biological, and optical parameters in the SLNC. An Ocean Optics USB2000 spectroradiometer was used to perform above-water measurements of remote sensing reflectance ($R_{rs}(0+)$). The radiometer had 2048 channels running from 360 up to 1100 nm. Measurements were performed using an optic cable connected to the radiometer. A Gershun tube at the end of the fiber was used to reduce the field-of-view (FOV) to an angle of 3°. $R_{rs}(0+)$ is measured using the protocol proposed by Mobley (1999) and recommended by Mueller et al. (2000). At each station, measurements were performed for downwelling irradiance $E_d(0+)$ using a Spectralon plate, for upwelling radiance $L_u(0+)$ with an azimuth viewing direction of 135° from the sun and a zenith angle of 40°, and for sky radiance $L_{sky}(0+)$. At least 10 measurements of each radiance or irradiance were averaged at every station. $R_{rs}(0+)$ was calculated according to Mobley (1999) by:

$$R_{rs}(0+) = \frac{L_w(0+)}{E_d(0+)} = \frac{L_u(0+) - \rho L_{\mathrm{sky}}(0+)}{E_d(0+)} \quad (1)$$

where $L_w(0+)$ is the water-leaving radiance, and ρ is the proportionality factor that relates the radiance measured when the detector views the sky to the reflected sky radiance measured when the detector views the sea surface. The value of ρ depends on solar zenith angle, wind speed, and cloud coverage. Under non-cloud conditions and wind speed less than 10 m s^{-1}, ρ is not wavelength-dependent, and for wind speed < 5 m s^{-1}, $\rho = 0.028$ (Mobley 1999).

Turbidity profiles were measured with a SeaBird SBE 19 CTD equipped with a Seapoint Turbidity Meter which detects light scattered by particles from a 0.88-μm wavelength light source. The sensor was factory adjusted for consistent response to Formazin Turbidity Standard measured in Formazin Turbidity Unit (FTU). Such a sensor, also called optical backscatter sensor (OBS) or nephelometer, is known to provide turbidity measurements proportional to sediment concentrations at low values, the proportionality coefficient varying between sites because it depends on particle shape, roughness, index of refraction, and particle size (Bunt et al. 1999; Jin et al. 2001). In coral reef lagoons, where various origins of particles provide a multi-modal particle size distribution, Bunt et al. (1999) suggest to interpret the nephelometer response preferentially as that of finer sediments. Here, the measured turbidity values are given in FTU. In the absence of accurate calibration in the lagoon of New Caledonia, we assume that backscatter sensors have a linear response to SPM concentration below 10 g l^{-1} (Bunt et al. 1999), that calibration differences between individual nephelometers are negligible (Larcombe et al. 1995), and that their sensitivity is about 1 FTU for 1 mg l^{-1} in coastal waters (Larcombe et al. 1995; Wass et al. 1997; Jin et al. 2001). The modeled fine sediment concentrations can thus be directly compared with the measured turbidity values. For future research, some parameters of the model will require a reliable calibration of that sensor as discussed at the end of this paper.

Finally, wind was continuously recorded every 10 min at one station in the middle of the lagoon to constrain the model (see Fig. 1).

Satellite data

A key element of this study is the availability of concurrent remote sensing and in situ data. We coordinated with the schedulers of the Landsat ETM + acquisitions to ensure that the satellite was turned on at the time of field surveys which were planned during the Landsat overpasses (Path/Row 81/75), every 16 days, during September–October 2002. To our knowledge, this is the first time that this has been made possible in a coral reef context. The Landsat 7 data with the least cloud coverage over the SLNC during this period was acquired on October 23, 2002 at 9h39 local time (October 22, 2002 at 22h39 GMT). Concurrent field measurements (turbidity profiles and in situ remote sensing reflectances) were performed within the lagoon at ± 2 h of the satellite overpass. The total radiance image was converted in top-of-atmosphere (TOA) reflectance using the standard coefficients and methods provided by the Landsat 7 Science Data Users handbook (http://ltpwww.gsfc.nasa.gov/IAS/handbook/handbook_toc.html).

Atmospheric correction

Concurrent in situ $R_{rs}(0+)$ data enabled us to explicitly calibrate the total radiance measured by the satellite (atmosphere, water column, and sea surface reflection) into remote sensing reflectance. In satellite observations of turbidity, the background intensity of light scattered by the atmosphere including the aerosols is greater than the light scattered by the suspended particles at concentrations below $\sim$3 mg l^{-1} (Sydor 1980). Therefore, the quality of atmospheric corrections is of primary importance in coastal waters to accurately estimate the remote sensing reflectance at sea level, and thus the concentration of suspended particles or the turbidity. However, accurate atmospheric correction in coastal environments is tricky because land, urban coastal areas, and oceanic environments co-exist. Spatial homogeneity of atmospheric conditions may not hold over areas of only a few square kilometers (Hu et al. 2000, 2001). In coastal environments, it is then more efficient and secure to rely on concurrent data to fine tune locally the correction of the image, even empirically. Once the image is calibrated in $R_{rs}(0+)$, it is possible to apply directly the relationship turbidity-$R_{rs}(0+)$ computed with a training set of in situ point data to obtain a gridded image of turbidity.

Model for transport of fine suspended particulate matter

The model for fine suspended sediment transport used in the present study is fully described in Douillet al. (2001). Below, we only give the necessary points relative to the formulation that is tentatively calibrated further. For modeling purposes, several classes of particles may be distinguished among suspended particles from their local grain-size distribution, each of them being characterized by a representative settling velocity or diameter. In the

latter case, a fall velocity (W_{Si}) may be calculated from Stokes' formula for particles with diameter less than 100 μm or from alternative equations such as Hallermeier's (1981) for silts and sands. The general transport equation for the concentration, denoted C_i, of a class of particles is given by:

$$\frac{\partial C_i}{\partial t}+\frac{\partial (uC_i)}{\partial x}+\frac{\partial (vC_i)}{\partial y}+\frac{\partial [(w-W_{si})C_i]}{\partial z} = \frac{\partial}{\partial x}\left(K_h\frac{\partial C_i}{\partial x}\right)+\frac{\partial}{\partial y}\left(K_h\frac{\partial C_i}{\partial y}\right)+\frac{\partial}{\partial z}\left(K_z\frac{\partial C_i}{\partial z}\right) \quad (2)$$

where u, v, and w are the x, y, and z velocity components; and K_h and K_z are the horizontal and vertical eddy diffusivities of particles, respectively. The horizontal eddy diffusivity of particles is considered as constant (0.002 m^2 s^{-1} in this study). The vertical eddy diffusivity of particles, K_z, is considered to be partially proportional to the vertical eddy viscosity N_z according to:

$$K_z=\frac{N_z}{\sigma_c} \quad \text{from the bottom up to depth } Z_n \text{ at which } N_z \text{ is maximum} \quad (3a)$$

$$K_z=\left.\frac{N_z}{\sigma_c}\right|_{z=Zn} \quad \text{from } Z_n \text{ up to the surface} \quad (3b)$$

where σ_c is the Schmidt number.

As can be seen in the above equations, the transport model strongly relies on velocity and turbulence fields which are provided by a hydrodynamic model. The hydrodynamic model used in this study involves a 2D depth-averaged model (Douillet 1998) which calculates the free surface elevations resulting from the tide propagation, and a full 3D model which uses results of the 2D model (Lazure and Salomon 1991). The influences of temperature and salinity variations on water density are not considered in the present version of the model.

At opened lateral boundaries, a Neumann condition is imposed in the case of an outgoing flux, and a value of concentration is imposed in the case of an inflow flux. At the sea surface (respectively, at the bottom), the condition expresses the flux of particles between the water column and the atmosphere (respectively the sea floor) with:

$$\left(K_z\frac{\partial C_i}{\partial z}-W_{si}C_i\right)_{\text{surface}}=0 \quad (4a)$$

$$\left(K_z\frac{\partial C_i}{\partial z}-W_{si}C_i\right)_{\text{bottom}}=D_i-E_i \quad (4b)$$

where D_i and E_i are the exchange rates of particles through deposition and erosion, respectively. The deposition rate formula (Krone 1962) is based on the assumption that a particle reaching the bottom has a probability of remaining there that varies between 0 and 1 as the bed shear stress (τ) varies between a critical shear stress for deposition τ_{cdi} specific to the class i of particles considered and zero. Over consolidated bottoms, the erosion rate E_i, expressed in kg m^{-2} s^{-1}, depends on the excess of τ as compared to a critical value for erosion denoted τ_{cei} following (Partheniades 1965):

$$E_i=ke_i\left(\frac{\tau}{\tau_{cei}}-1\right)\tau>\tau_{cei} \text{ and } \mathrm{E}=0 \text{ for } \tau<\tau_{cei} \quad (5)$$

where ke_i is the erosion rate coefficient for class i of particles. ke_i depends on the soil consolidation.

Settings of the SPM transport model

In the absence of measurements for grain-size distribution within the water column, only one single class of particles (7-μm diameter) is considered in the numerical simulations. This diameter corresponds to the more significant population of fine mud in the surface sediments in the Dumbéa Bay, near Nouméa (O'Callaghan 1999). We assume that this population is representative of the fine sediments in the lagoon whose concentrations are estimated by OBS or by remote sensing. Three parameters must be calibrated for the considered class of particles: the critical shear stresses τ_{cd} and τ_{ce}, and the erosion rate coefficient ke.

As in Douillet et al. (2001), τ_{cd} and τ_{ce} are assumed to be equal, meaning that there is always either net deposition or net erosion over a given area, except over the reefs where erosion of fine particles does not occur. Under the assumption that the surface sediment distribution is forced mainly by trade winds (e.g. Larcombe and Woolfe 1999), the critical shear stress τ_{cr} was set as the value of bottom shear stress at the limit of the mud-dominated areas for mean tidal and wind forcing ($\tau_{cr}=0.017$ Pa). Our estimate of the critical shear stress is more consistent with continental margins than for estuaries or coastal zones (see e.g. Dade et al. 1992; Thomsen and Gust 2000; Schaaff et al. 2002).

Douillet et al. (2001) assumed that the erosion rate coefficient was proportional to the local volume fraction of mud in the surface sediments, denoted P_{mud}, according to:

$$ke=ke_c\cdot P_{\text{mud}} \quad (6)$$

where ke_c is a fitting parameter. A bulk initial value of ke_c, hereafter denoted $ke_{c\ init}$, was set for the entire lagoon for these particles, with $ke_{c\ init}=7.5\times10^{-5}$ g m^{-2} s^{-1}, so that deposition and erosion fluxes compensate over a tidal cycle under the mean tidal and wind forcings. This setting did not take into account the spatial variations in soil consolidation. ke_c may be estimated from field measurements at a finite number of stations, but due to the high heterogeneity of soils and sediment distribution (Debenay 1987; Chardy et al. 1988), field measurements would only provide an imperfect distribution, with many gaps in a large lagoon. In this study, the synoptic distribution of turbidity obtained from Landsat 7 is used to estimate the distribution of the fitting parameter ke_c or, in other words, to estimate the distribution of the erosion rate coefficient.

Simulation of SPM transport

Hydrodynamics were modeled taking into account the two main physical factors controlling the current regime: tide (constituents M_2 and S_2) and wind (Douillet 1998). The conjunction of M_2 and S_2 enables modeling of neap tides and spring tides. Wind-speeds recorded at Maître islet have been used (Fig. 1). Rainfall was minimal in September-October 2002 so that the negligible river freshwater inputs were not considered in the simulation. To minimize the boundary condition influence, an area larger than the study area was modeled. For initial conditions, the circulation model was activated 1.5 month before the satellite overpass, i.e. in early September 2002, when the winds were weak. The SPM transport model was initiated 23 days before the date of study, during another period of weak winds. SPM concentration was uniformly initiated in the study area at a value of 0.2 mg l^{-1}, which has a limited influence on the final results because wind velocity had increased steadily during several days before October 23, 2002. During the week before October 23, 2002, trade winds were blowing with a direction varying between 90° and 150° and a velocity of 7 to 12 m s^{-1}. During the night of 22 to 23 October 2002, wind decreased to 2 m s^{-1}. The tide during the previous days was spring tide and a high tide occurred at 9h12 local time in Nouméa, half an hour before the satellite overpass (9h39).

The horizontal grid size of the model is 500 m and the water column is divided into 10 σ-depth levels. The calculation time step is 40 s in order to avoid numerical instability induced by the settlement of particles.

Results and discussion

Relationship between turbidity and spectral reflectance in the lagoon of New Caledonia

Simultaneous measurements of $R_{rs}(0+)$ and of vertical turbidity profiles were performed at 75 marine stations

over the SLNC from June 2002 to January 2003. A full analysis of these data indicates that the best fit and sensitivity between turbidity and hyperspectral reflectance occurs (*i*) at wavelengths around 565 nm, (*ii*) for turbidity averaged from the surface down to a depth of about 5 m, and (*iii*) for stations with a water depth greater than about 14 m, or greater than 10.5 m in case of a surface turbidity greater than 1 FTU. Thus three populations were considered: (1) 40 'deep' stations (i.e. verifying the above criterion *iii*) that were not performed on October 23, 2002, (2) 14 'deep' stations performed on October 23, 2002 at ±1h40 from the Landsat 7 ETM+ overpass, and (3) 21 'shallow' stations. In the present paper, population 1 was used to establish an empirical relationship between turbidity and spectral reflectance independently from the image, population 2 was used to test the turbidity estimates from ETM+ data, and population 3 was not used because the bottom influence may be larger than the turbidity influence on above-water reflectance over shallow waters. The location of stations of population 2 and of stations of October 22, 2002 within population 1 is shown in Fig. 1.

The reflectance spectra of the training set of data (population 1) are shown in Fig. 2. From the spectral measurements of $L_w(0+)$ and $E_d(0+)$, the equivalent-satellite remote sensing reflectance for band k of Landsat 7 ETM+, namely $R_{rsL7,k}$, was calculated according to:

$$R_{rsL7,k} = \frac{\int_{\lambda_{1k}}^{\lambda_{2k}} L_w(\lambda) S_k(\lambda) d\lambda}{\int_{\lambda_{1k}}^{\lambda_{2k}} E_d(\lambda) S_k(\lambda) d\lambda} \quad (7)$$

where $S_k(\lambda)$ is the radiometric sensitivity of band k that extends from λ_{1k} up to λ_{2k}.

Different types of regression (linear, log-linear, exponential, polynomial, power) were performed for bands 1, 2, and 3 and for the band ratios. The best fit was obtained between $R_{rsL7,2}$ (R_{rs} in ETM+ band 2, from 525 to 605 nm) and the turbidity averaged over the uppermost 5 m (Fig. 3). The empirical relationship for the regression ($r^2 = 0.946$, $n = 40$) is:

$$\text{Turb} = -416782 R_{\text{rsL7,2}}^3 + 17913 R_{\text{rsL7,2}}^2 - 35.299 R_{\text{rsL7,2}} + 0.2147 \quad (8)$$

where *Turb* is expressed in FTU and $R_{rsL7,2}$ is expressed in sr^{-1}. This relationship is valid for turbidity between 0.2 and 2.7 FTU.

The choice of ETM+ band 2 in the inversion procedure is the same as in Khorram et al. (1991) and Tassan (1987) who suggested using Landsat 5 Thematic Mapper band 2 (TM2) for waters of low turbidity, whereas other bands are more suitable for more turbid waters: TM3 is preferred for SPM concentration above around 1 mg l^{-1} by Tassan (1987); TM2 or TM3 for SPM concentration between 5 and 50 mg l^{-1} by Dekker et al. (2002); TM2/TM3 for SPM concentration between 40 and 380 mg l^{-1} by You and Hou (1992) and between 5 and 100 mg l^{-1} by Topliss et al. (1990); and TM4 for SPM concentration between 30 and 200 mg l^{-1} by Ritchie et al. (1990).

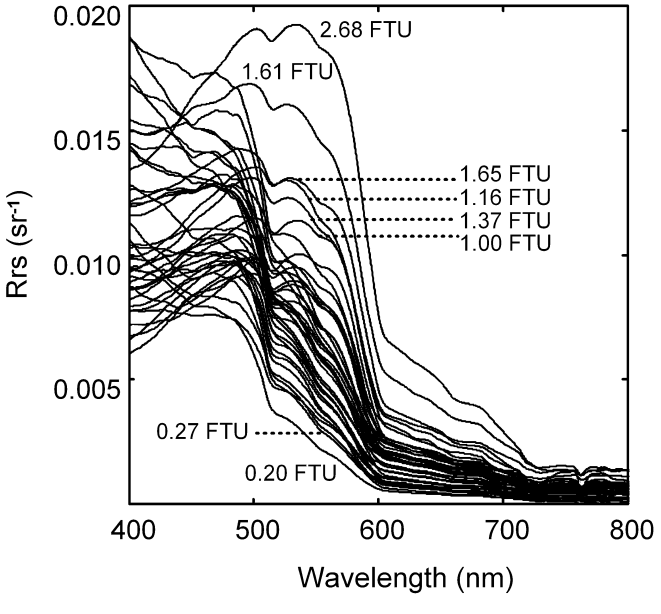

Fig. 2 Above-water remote sensing reflectance (*Rrs*) at 40 'deep' stations (water depth >14 m, or water depth >10.5 m and turbidity >1 FTU) measured between June 28, 2002 and January 14, 2003 in the southwest lagoon of New Caledonia (SLNC)

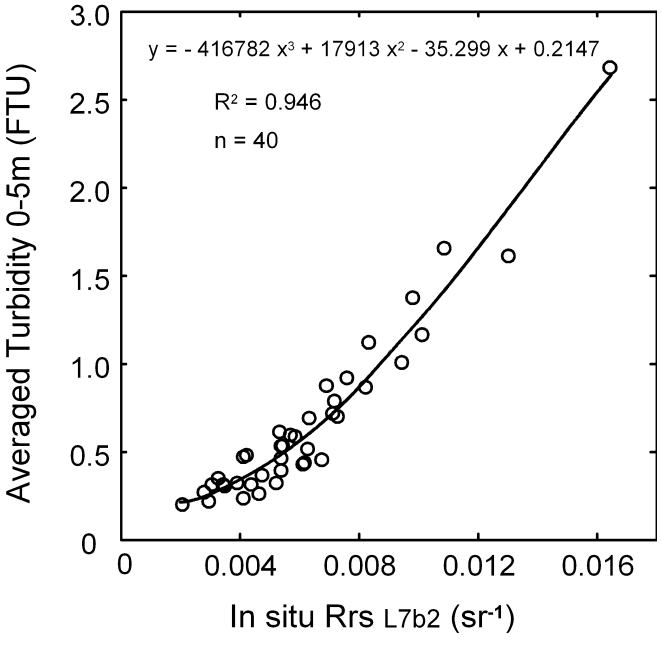

Fig. 3 Empirical relationship between equivalent remote sensing reflectance in Landsat 7 ETM+ band 2 ($R_{rsL7,2}$) and turbidity averaged from the sea surface down to 5-m depth ($R^2 = 0.946$, $n = 40$)

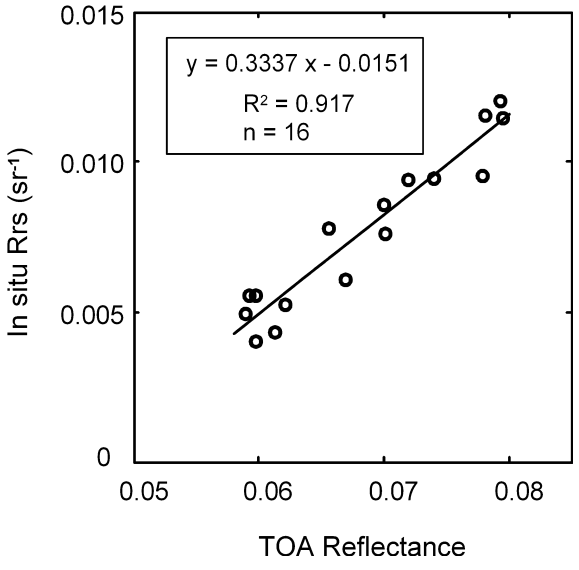

Fig. 4 Regression relationship between in situ R_{rs} at sea level and top-of-atmosphere (TOA) reflectance for Landsat 7 ETM + band 2 on October 23, 2002 at 9h39 local time ±1h40

Atmospheric correction

Sixteen in situ $R_{rs}(0+)$ spectra (unit sr^{-1}), that were obtained at ±1h40 of the October 23rd Landsat overpass, were used to calibrate empirically the band 2 TOA reflectance ($R_{L7,2}$ (TOA), unitless) signal into $R_{rsL7,2}(0+)$ using a linear regression (Fig. 4). We obtain ($r^2 = 0.917$, $n = 16$):

$$R_{rsL7,2}(0+) = 0.3337 R_{L7,2}(TOA) - 0.0151 \quad (9)$$

This empirical correction accounts for most of the atmospheric and geometrical effects. Differences in time (±1h40) and different spatial resolution (Landsat pixels cover 900 m^2, in situ measurement covers ~1 m^2) likely induce noise of unknown magnitude in the relationship.

Turbidity distribution on October 23 from Landsat 7 ETM +

Remote sensing reflectances were converted into turbidity using Eq. (8). The resulting map of turbidity over the entire SLNC is presented in Fig. 5. Maximum turbidities occur adjacent to the coastline, especially in the bays. Turbidity is lower in the southern part of the lagoon than in its northern part due to exports from the Nouméa bays, with the resulting currents flowing to the northeast. Remember that the empirical inversion relationship is valid only over 'deep' zones (those making up population 1 of marine stations), i.e. for water depth >14 m, or depth >10.5 m if local turbidity >1 FTU. Shallow areas, over which the inversion procedure is expected to artificially overestimate turbidity because of an enhanced reflectance due to bottom influence, were masked.

Calibration of the erosion rate coefficient ke

A first numerical simulation of SPM transport in October 2002 was performed with a ke_c parameter uniformly distributed over the lagoon. From direct visual comparison of the turbidity field derived from Landsat 7 (Fig. 5) and SPM concentration field on October 23, it was evident that the differences from one lagoon region to another were substantial. The difference between satellite and modeled suspended loads was small in the main part of the lagoon (underestimation by the model of about 15%) but higher close to the coast and in the bays. The relatively low simulated SPM concentration in

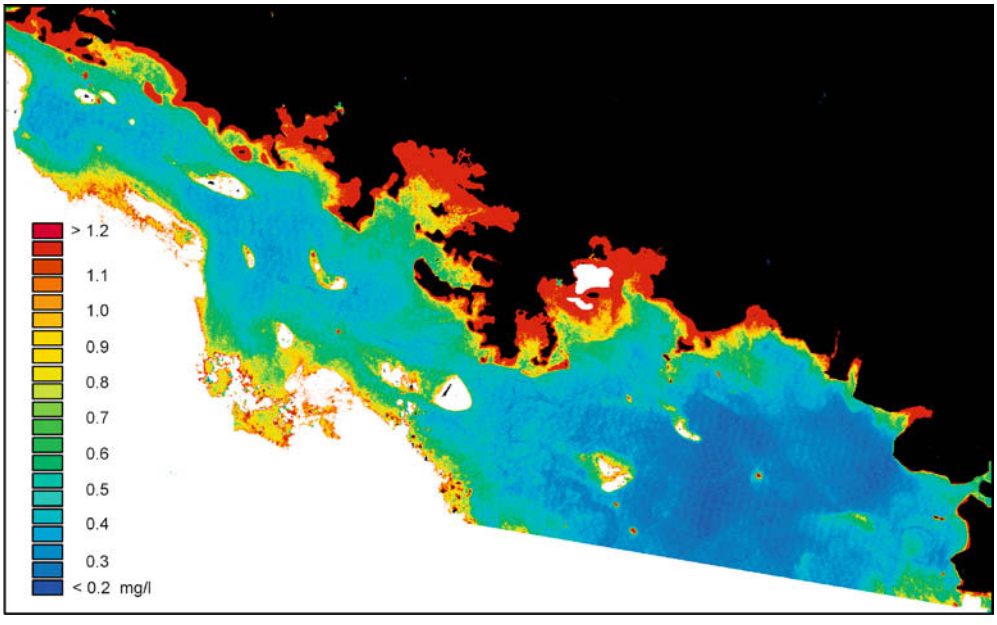

Fig. 5 Turbidity (in FTU) field calculated from Landsat7 ETM + band 2, on October 23, 2002 at 9h39 local time (October 22, 2002, 22h39 GTM)

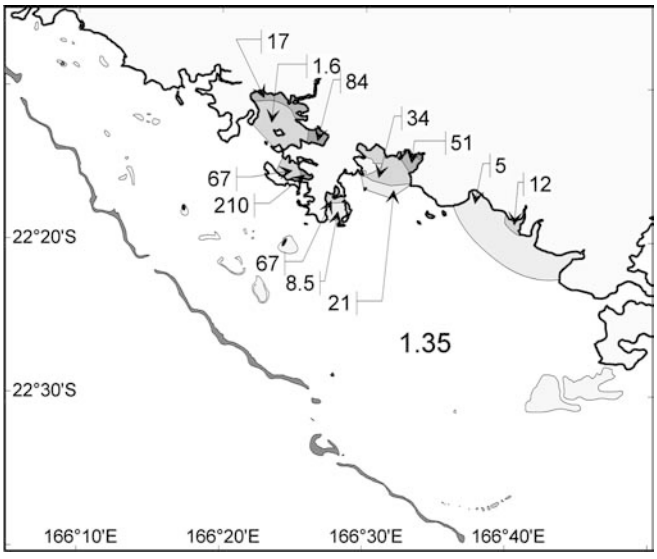

Fig. 6 Ratio between the estimated erosion rate coefficient ke_c per zone and the initial bulk erosion rate coefficient $ke_{c\ init}$

the bays results from low rates of erosion, themselves explained by poor estimates of local parameters τ_{ce} and ke_c, and lack of wind waves forcing in the model. Wind waves, when present, should increase the bed shear stress over shallow water and modulate the estimate of τ_{ce} proposed by Douillet et al. (2001). This will be investigated in a future study with a wave model coupled to the hydrodynamic model. Here, we investigated the distribution of the erosion rate coefficient, assuming that the critical shear stress for erosion was known. Tests were performed to replace the uniform value of ke_c over the entire lagoon by a distribution of ke_c designed to produce good agreement between the simulated SPM concentrations and turbidity measured at sea or estimated by Landsat 7.

The actual value of the erosion rate coefficient is related to the cohesion of the surface sediments. As the initial bulk erosion rate coefficient of 7.5×10^{-5} g m^{-2} s^{-1} provided SPM concentrations in the lagoon slightly less than the turbidity measured at sea, we first increased the value of this bulk coefficient until the simulated and measured values were in good agreement in the main part of the lagoon. This was achieved with $ke_c = 1.35\times ke_{c\ init}$. Secondly, several zones, each of them with a uniform ke_c value, were defined in the bays and along the coast. The limit of the different zones was defined by visual comparison between the turbidity distribution from Landsat 7 and the one simulated for October 23 2002. The value of the fitting parameter was tuned to reach good agreement between (1) the calculated profiles of SPM concentration with the in situ depth-profiles of turbidity, and (2) the histograms of turbidity provided by Landsat 7 and of modeled SPM concentration. The final zonation after 20 iterative tests and the corresponding value of ke_c per zone compared to $ke_{c\ init}$ are presented in Fig. 6. The chosen distribution of the

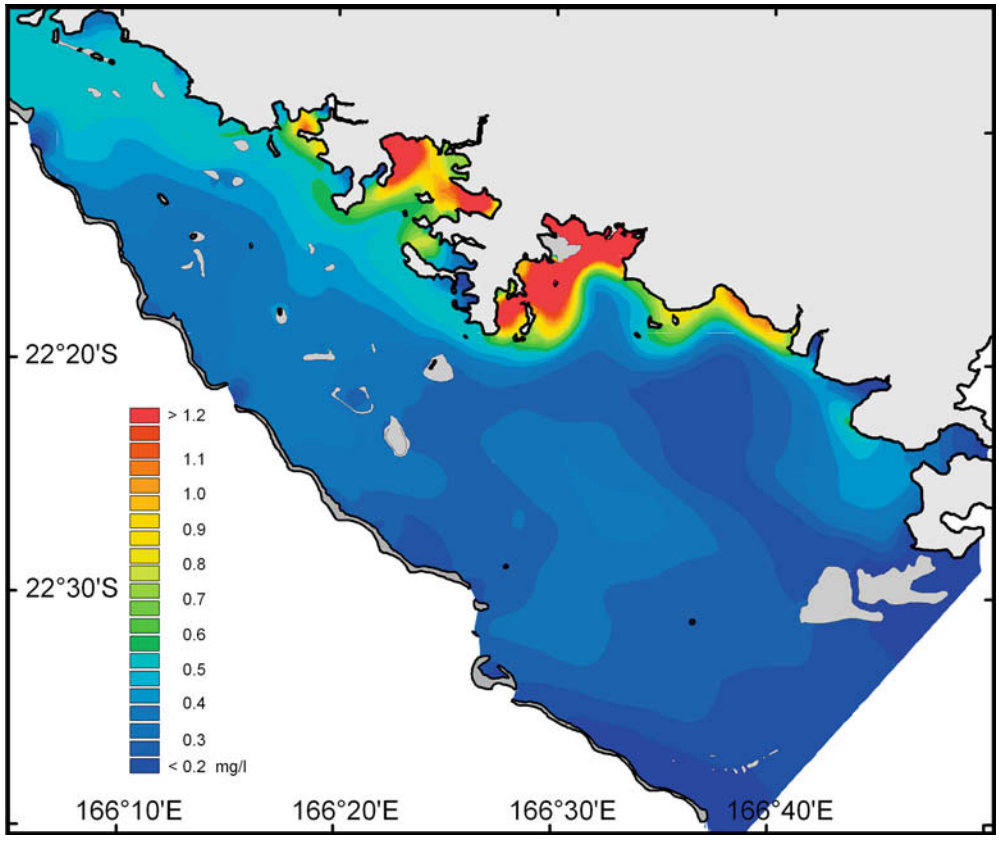

Fig. 7 SPM concentration (in mg l^{-1}) field obtained by numerical model for October 23, 2002 at 9h39 local time (October 22, 2002, 22h39 GTM)

Table 1 Values of $R_{rsL7,2}$ and of turbidity averaged from the surface down to 5 m depth at 14 'deep' stations constituting population 2, and at 2 shallow stations (*in italic*) on October 23, 2002. Estimates of $R_{rsL7,2}$, of turbidity from TOA $R_{L7,2}$ and of SPM concentration calculated by the model are compared to the measurements

Station	Long. WGS84	Lat. WGS84	Depth (m)	Time GMT + 11	$R_{rsL7,2}$ *in situ* (sr^{-1})	$R_{rsL7,2}$ from TOA $R_{L7,2}$ (sr^{-1})	Diff. L7-in situ R_{rs} (%)	Aver. in situ Turb. 0–5 m (FTU)	Aver. $Turb_{L7,2}$ 0–5 m (FTU)	Diff. L7-in situ Turb. (%)	SPM conc. below surf. ($mg\ l^{-1}$)	Diff. model/ in situ (%)
P12	166.6465	−22.3405	30.0	8h04	0.0049	0.0046	−7.1	0.416	0.385	−7.5	0.233	−44.0
P04	166.6730	−22.3153	16.5	8h17	0.0078	0.0068	−12.6	0.860	0.665	−22.7	0.855	−0.6
R02	166.6647	−22.3117	19.5	8h25	0.0055	0.0048	−12.9	0.440	0.413	−6.1	0.544	+23.8
R03	166.6000	−22.3272	25.3	8h44	0.0056	0.0047	−15.5	0.465	0.398	−14.3	0.475	+2.1
B24	166.5337	−22.3220	27.1	9h01	0.0040	0.0048	+21.2	0.300	0.413	+37.7	0.309	+2.9
B16	166.5153	−22.2845	22.0	9h15	0.0094	0.0089	−5.4	1.005	1.021	+1.7	1.082	+7.7
B08	166.5210	−22.2672	17.8	9h24	0.0120	0.0114	−5.7	1.728	1.506	−12.8	1.242	−28.1
B03	*166.5487*	−22.2505	*8.2*	*9h35*	*0.0116*	*0.0110*	*−5.2*	*1.911*	*1.422*	*−25.6*	*1.857*	*−2.8*
R04	166.5092	−22.2762	19.1	9h48	0.0096	0.0109	+14.0	1.329	1.407	+5.9	1.339	+0.8
N04	166.4627	−22.2870	10.8	10h02	0.0114	0.0114	−0.1	1.806	1.522	−15.7	1.082	−40.1
N20	166.4643	−22.2973	15.0	10h13	0.0095	0.0096	+1.2	1.217	1.147	−5.7	1.409	+15.8
N30	166.4668	−22.3117	14.4	10h26	0.0061	0.0072	+18.8	0.644	0.733	+13.8	0.750	+16.5
N43	166.4315	−22.3205	20.6	10h43	0.0043	0.0054	+24.8	0.314	0.473	+50.7	0.411	+30.9
N44	166.3832	−22.2955	24.6	10h57	0.0052	0.0056	+7.3	0.418	0.505	+20.6	0.448	+7.1
D46	166.3855	−22.2053	15.5	11h13	0.0076	0.0083	+9.1	0.670	0.914	+36.4	0.919	+37.2
D47	*166.3922*	*−22.1987*	*10.3*	*11h20*	*0.0086*	*0.0083*	*−3.5*	*0.922*	*0.905*	*−1.9*	*0.982*	*+6.5*

erosion rate coefficient, with greater values in the bays and near the river mouths than in the main part of the lagoon, suggest that the deposited sediments should be more easily resuspended in these areas. The absolute values of the erosion rate coefficient (from 10^{-4} up to 63×10^{-4} g m^{-2} s^{-1}) are slightly less than those indicated in the literature for, e.g., estuaries (Brenon 1997).

The resulting distribution of SPM concentration just below the sea surface, at a depth of 5% of the total water depth, for October 23 is presented in Fig. 7.

Comparison between image and in situ measurements

$R_{rsL7,2}$ and Landsat-derived turbidity levels were compared to those measured at sea at 14 different stations making up population 2 of stations (Table 1). The relative difference between the $R_{rs}(0+)$ values measured at sea and those calculated from Landsat TOA reflectances is 10.3% when averaged over the 14 stations, and it is greater than 20% at 2 stations, B24 and N43, where the measured R_{rs} are the lowest ($\sim$0.004 sr^{-1}, see Table 1). Over the 14 stations, the difference of 10% is of the order of the uncertainty in the reflectance measurement.

The averaged difference between turbidity estimated from Landsat and turbidity measured at sea is 17.5% at the 14 stations. Five out of 14 stations (N43, B24, D46, P04, B03) present relative difference greater than 20% (Table 1) that can easily be explained:

- The greatest relative differences are obtained at stations N43 (50.7%) and B24 (37.7%) where turbidity is minimum ($\sim$0.3 FTU), making the use of the empirical relationship (Eq. 8) more uncertain near the limit of its range of validity. However, the absolute differences of 0.11 and 0.16 FTU between measured and satellite-derived turbidities are very low at these stations.
- The difference at Stn. D46 (36.4%) may be explained by the local strong vertical stratification (see Fig. 8 introduced in the next section). Indeed, the empirical regression in this paper relates $R_{rsL7,2}$ and turbidity averaged over the upper 5 m, while the depth of light penetration depends on the turbidity itself. At Stn. D46, Landsat-derived turbidity is closer to turbidity averaged over the upper 3 m (0.714, difference of 28%), 10 m (0.737, difference of 24%) or 12 m (0.906, difference of 0.8%) than turbidity averaged over the upper 5 m.
- The Landsat-derived turbidity at Stn. B03 underestimates by 25.6% the measured turbidity. Even if water depth is shallow at B03 (8 m), the error cannot be assigned to bottom influence because this would likely infer an overestimation of reflectance and turbidity. This difference cannot be assigned to an atmospheric correction error either, since satellite-derived and in situ R_{rs} values differ only by 5.2%. It appears that the empirical relationship (Eq. 8) does not apply well at Stn. B03. Differences in the optical characteristics of

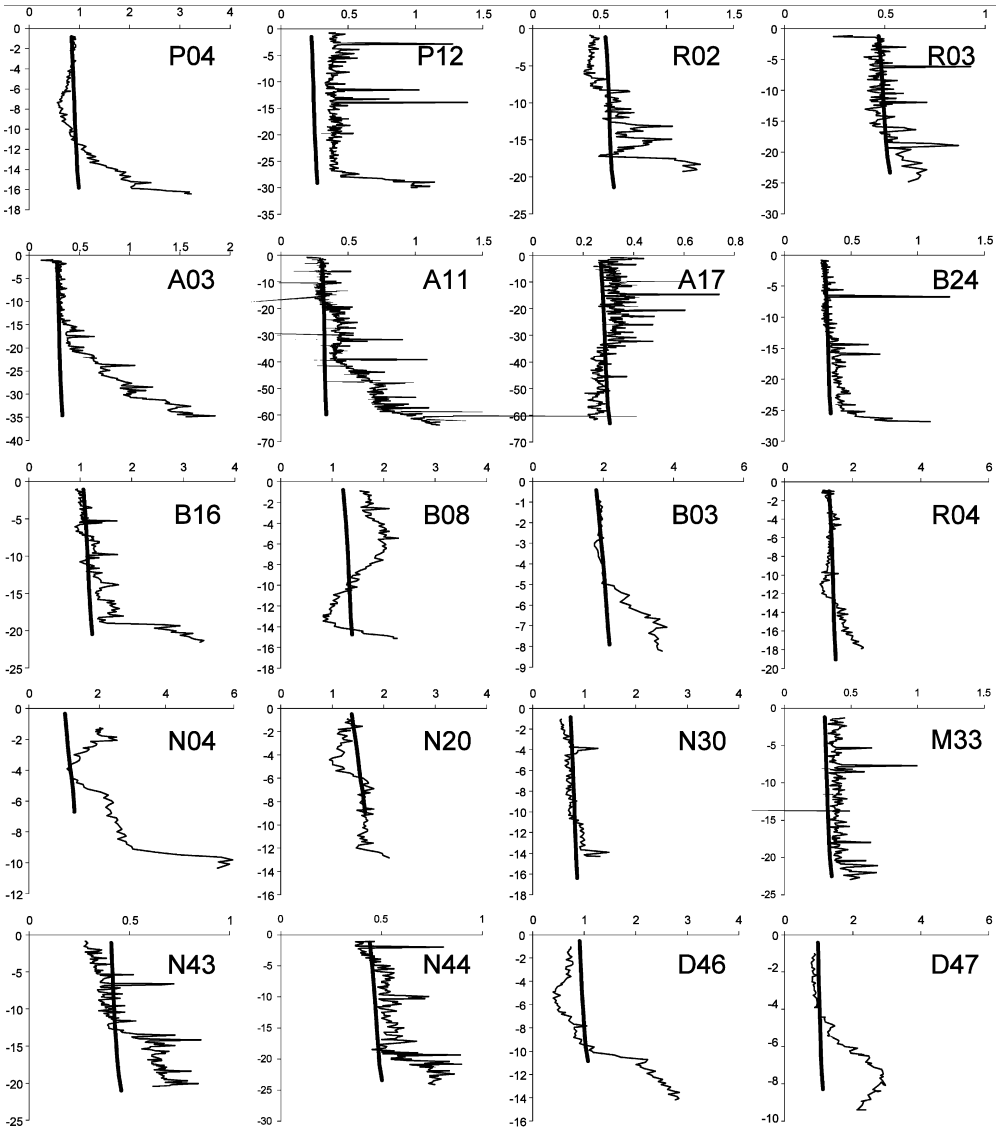

Fig. 8 Profiles of turbidity (measurements, in FTU) and of suspended particulate matter concentration (*bold*: numerical simulation, in mg l^{-1}) at 20 stations on October 23, 2002, 9h40 local time ± 2 h. Water depth from the surface is given with *negative values*

suspended particles near the Coulée river mouth (Boulari Bay, see Fig. 1), or a lack of in situ measurements with turbidity greater than 1.5 FTU in the training set of data, likely explain this discrepancy, thus making the turbidity estimate uncertain outside the range 0.3–1.5 FTU.

– The underestimation of turbidity at Stn. P04 (22.7%) is mainly assigned to the underestimation of R_{rs} (12.6%) by Landsat.

These discrepancies should not hide that an averaged difference of 17.5% between Landsat-derived turbidity and measurements at 14 stations is a very good result. Previous published results are generally worse: 35% differences were observed in highly turbid waters (Doxaran et al. 2002), and 25% in less turbid waters of river plumes (Ouillon 2003). We assume that this is because turbidity is an indirect and optical estimation of the suspended particles, and is thus better correlated with reflectance than the dry weight of particles.

Comparison between simulation and in situ measurements

The vertical profiles of measured turbidity on October 22 and 23 were used to fit locally some values of ke_c in complement to the field and Landsat data of October 23 (Figs. 8 and 9). If we assume that SPM concentration from the model and in situ turbidity are equal despite their different units, the difference between both values is 16.7% in average for 14 stations surveyed 23rd October (Table 1). Six out of 14 points show a difference greater than 20% (P12, R02, B08, N04, N43, D46) (Table 1). The analysis of the discrepancies for October 23 (Table 1 and Fig. 8) or for October 22 (Fig. 9) points out failures of the model: (1) significant differences between measurements and simulations are obtained when there is a benthic nephelo layer (A03 and A11 in a canyon) or a surface plume (N04), or, more generally, when there is a stratification in

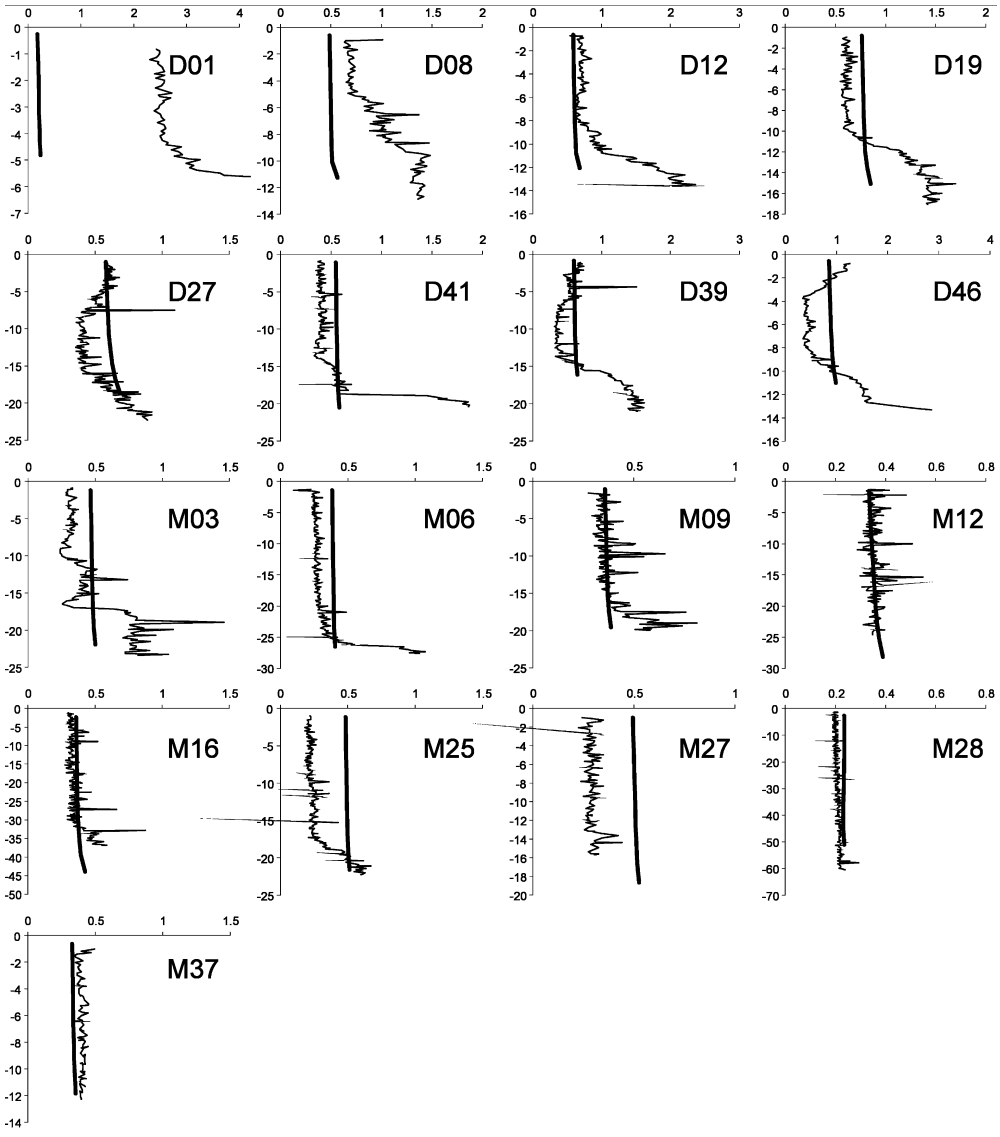

Fig. 9 Profiles of turbidity (measurements, in FTU) and of SPM concentration (*bold*: numerical simulation, in mg l^{-1}) at 16 stations on October 22, 2002 in the morning

temperature or salinity (e.g. B08, N43, D46); (2) significant differences are also obtained in the bays (N04, D01, D08). The model fails to reproduce properly the vertical heterogeneity of turbidity because the temperature and salinity fields are not calculated in the present version and also because the estimate of vertical diffusivity of particles was not fitted here. Regarding the bottom of bays, the discrepancy is explained by the coarse mesh grid size (500 m), that does not allow proper simulation of the dynamics over a few enclosed meshes, and because wave forcing is not accounted for in the present calculation.

Comparison between simulation and image

The simulated distribution of SPM concentration (Fig. 7) shows the same general pattern as the satellite derived map of turbidity (Fig. 5): the waters are less turbid in the southern part of the lagoon than in the northern part, and main resuspension occurs in the bays and along the coast. In order to compare the two distributions, we calculated the ratio of Landsat derived turbidity versus SPM concentration at each point of the mesh grid for October 23, 2002 at 9h39 local time. A ratio close to one indicates a very good agreement and greater values indicate either that turbidity is overestimated by Landsat or that SPM concentration is underestimated by the model. The histogram of this ratio over the entire domain enables a full assessment of the differences between simulation and image (Fig. 10). It was used in the iterative procedure to fit the erosion rate coefficient in order to maximize the percentage of points with ratio between 0.9 and 1.1.

The best fitted set of erosion rate coefficients (Fig. 6) provides a histogram where 47.7% of points have a ratio between 0.7 and 1.3 and where 62.6% of points have a ratio between 0.5 and 1.5 (Fig. 10). The histogram also shows that 19.8% of points have a ratio greater than 2.5. These latter points are principally located in the very

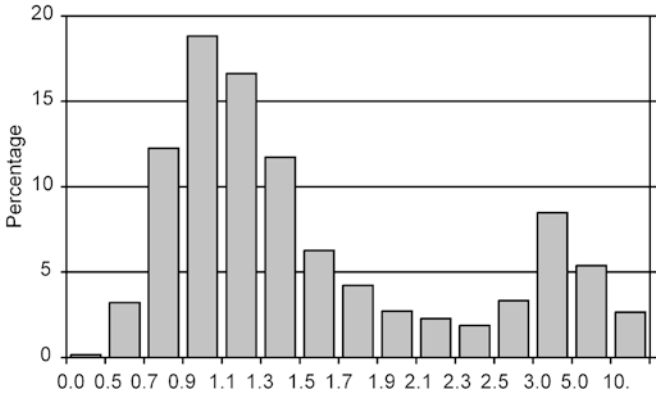

Fig. 10 Histogram of ratio "Landsat 7 turbidity/modeled SPM concentration" for October 23, 2002 at 9h39 local time over the entire common domain of Landsat image and of calculation. The vertical axis indicates the percentage of points in each bin

shallow areas (Fig. 11), essentially over the bright reef flats and white sand bottoms of back-reefs where the inversion is invalid. For the same reason but to a lesser extent, the inversion of Landsat data is assumed to slightly overestimate turbidity in the turbid bays since the bottom also contributes to the water-leaving radiance. The other points with high $ke_c/ke_{c\ init}$ ratio are essentially located in different bays with values of 34, 84, or 210 (see Fig. 6). In these areas the shear stresses calculated by the model were very low and were probably underestimated as noted above, and do not allow the resuspension of particles.

Turbidity patterns revealed by Landsat are closely linked to bathymetry, because bottom shear stress that is responsible for local resuspension decreases with increasing water depth. However, there are many differences between turbidity distribution and bathymetry that may be partly explained from the model results (see Figs. 1 and 5): (1) turbidity patterns in Boulari Bay differ from bathymetry because the water masses load high amounts of particles in the anticyclonic gyre of this bay that are transported over a few kilometers before settling down. Thus the satellite-derived turbidity field and bathymetry do not show the same gradients; (2) similarly, the greater turbidity in the northern part of the lagoon as compared to the southern part for equivalent depths is due to particles resuspended in Boulari and Dumbéa bays that are transported by wind and tidally induced currents; (3) several small plumes can be identified over the image whose patterns are very distinct from the local bathymetry, for example near the Pirogues river mouth, southeast of Mont Dore, and southwestward from Nouméa bays. The transport of resuspended particles by currents seems to be satisfactorily reproduced by the model, but the plumes are not. Different causes may explain this: river inputs, if any, were neglected in the simulation; resuspension is not well reproduced in the Nouméa bays, because significant causes of resuspension over small water depths, like waves, are not taken into account in the

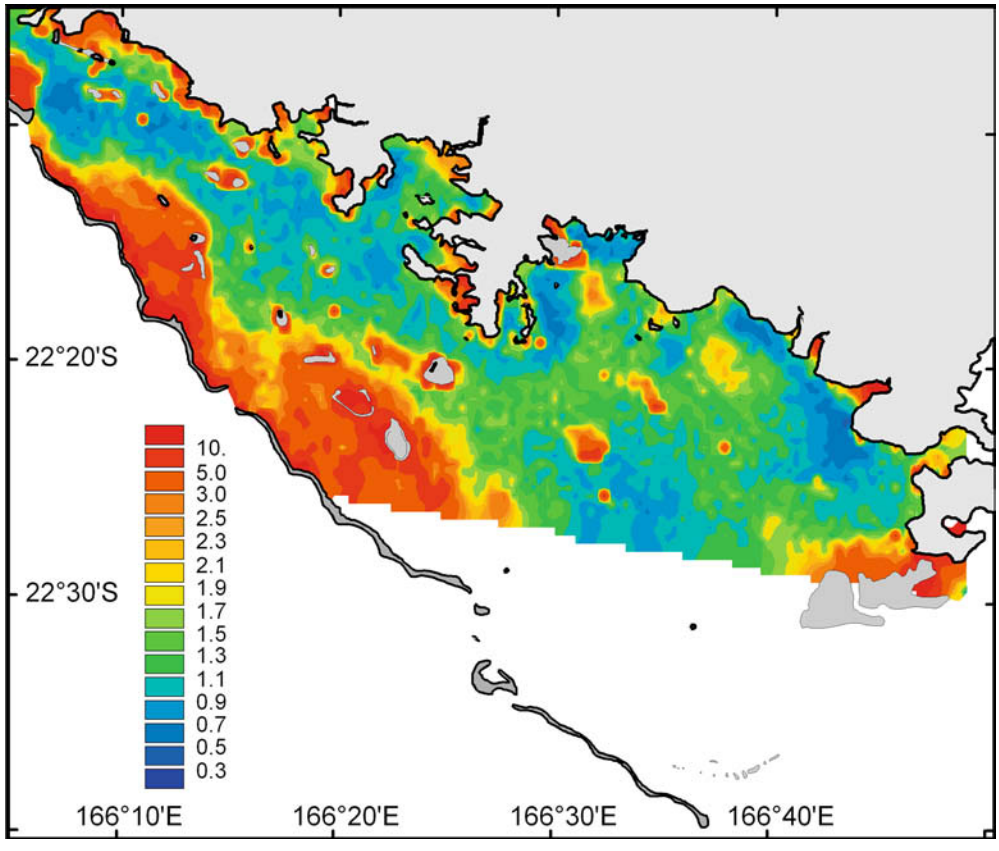

Fig. 11 Distribution of ratio "Landsat 7 turbidity/modeled SPM concentration" for October 23, 2002 at 9h39 local time

model; the plume that can be distinguished southeastward of Mont Dore could be attributed to other types of particles than sediments, since many narrow slicks (from about 1 to 3 m large) of cyanobacteria *Trichodesmium* were observed on October 23 in this area.

Future developments

Next steps for model improvements include the validation of the coefficients that were fitted for the situation of October 23, 2002. First, they need to be confirmed by considering other situations in time. Validation could be also achieved by local turbidity measurements near the bottom over homogeneous seabeds. Second, the values of the best-fit coefficients should be tentatively explained by or related to sedimentological or physical parameters such as the porosity of surface sediment, the relative amount of mud in a sand/mud mixture or the relative proportion in carbonate in a carbonate/terrestrial mixture.

In parallel to the continuation of the model calibration and validation, several improvements are required for field measurements, model development, and inversion of remote sensing data:

- In the present study, SPM concentrations are compared to turbidity measured by a Turbidity Meter, assuming a linear response of 1 FTU per mg l^{-1} at concentrations lower than 10 mg l^{-1}. A series of Turbidity Meter calibrations are required to account for grain-size variations, since the SLNC has non-homogeneous bottom sediments and varying hydrodynamic conditions. For that purpose, we intend to deploy a laser particle sizer in the field.
- The influence of wind-waves on sediment resuspension is a major relevant process that should be integrated in the model with two consequences (1) in the shallower and more exposed areas (e.g. bays), the bottom shear stress resulting from coupled currents and waves should be greater than those calculated only under the current influence (e.g. Soulsby 1997), increasing the estimation of the critical shear stress for erosion on the basis of the same physical reasoning; (2) to generate the same level of turbidity, erosion rate coefficients will decrease when the waves will be considered, especially over the shallower depths more sensitive to the wave action, thus diminishing the gap amongst the erosion rates within the lagoon.
- Inversion of turbidity from R_{rs} will require taking into account the bottom influence, especially over shallow waters. The vertical stratification of SPM concentrations, if any, could also be inverted from multispectral data (Ouillon 2003).

Conclusion

Despite the different improvements that can be expected in the field measurements, in the model, and in the satellite data inversion, the present study shows that remote sensing is a powerful tool to study the transport of suspended particles in a coral reef lagoon, and more generally in coastal zones with low suspended loads.

A main drawback of in situ measurements, as outlined by Puls et al. (1994), is that "*isoline maps of SPM concentrations from ship cruise data do not represent a (real) synoptic distribution, but a not well defined mixture of spatial and temporal information*." Satellite data give a synoptic estimation of the instantaneous field of concentration, but this synoptic view is restricted to a surface layer of a few meters thickness and to cloud-free conditions. A further restriction is that, during storms and cyclones, when local erosion and river inputs are maximum, the SPM distribution cannot be observed in real-time but only with some delays (Andréfouët et al. 2002). Numerical modeling *a priori* enables to calculate the synoptic three-dimensional distribution of SPM concentration, but it is restricted by the knowledge on the relevant processes, the boundary conditions, and the parameters involved in the process formulations.

A calibrated and validated numerical model is an excellent tool to understand and interpret the suspended particulate matter transport. It enables sensitivity studies, pointing to the processes that are relevant or not, and in what proportion. Every improvement of process representation may be tested and analyzed. Satellite data, in complement to field measurements, may help to adapt the coefficients of the model. Whereas field measurements can be used to tune the coefficients involved in the vertical profile of physical parameters (eddy diffusivity of particles, concentration, erosion rate coefficient, critical shear stress) and to finely determine some of these parameters at a reduced number of marine stations, the synoptic distribution provided by satellite data can be used to tune the horizontal variations of some coefficients (erosion rate, critical shear stress). A tuned model will bring new understanding regarding the particulate transport when the coefficients, once estimated from measurements or from remotely sensed data, will be related to the local sedimentology and to coral reef health.

Acknowledgements This study was supported by IRD (UR CAMELIA), by the French scientific Programme National Environnement Côtier (PNEC), by the French programme ZoNéCo, and by the French ACI 'Observation de la Terre' (programme BISSECOTE). NASA supported this work (grant NAG5-10908 to S.A.). P. Larcombe, J.-M. Froidefond, and B. Riegl are thanked for their helpful reviews. We are indebted to T. Arvidson for the scheduling of Landsat 7 acquisition in October 2002. The authors are also grateful to Captain S. Tereua of the O.R.V. CORIS. This is IMaRS contribution 054.

References

Alibert C, Kinsley L, Fallon SJ, McCulloch MT, Berkelmans R, McAllister F (2003) Source of trace element variability in Great Barrier Reef corals affected by the Burdekin flood plumes. Geochim Cosmochim Acta 67:231–246

Andrefouët S, Mumby PJ, McField M, Hu C, Müller-Karger FE (2002) Revisiting coral reef connectivity. Coral Reefs 21:43–48
Baban SMJ (1995) The use of Landsat imagery to map fluvial sediment discharge into coastal waters. Mar Geol 123:263–270
Booth JG, Miller RL, McKee BA, Leathers RA (2000) Wind-induced bottom sediment resuspension in a microtidal coastal environment. Cont Shelf Res 20:785–806
Brenon I (1997) Modélisation de la Dynamique des Sédiments Fins dans l'Estuaire de la Seine. PhD Thesis report, Univ Bretagne Occ, p 204
Bunt JAC, Larcombe P, Jago CF (1999) Quantifying the response of optical backscatter devices and transmissometers to variations in suspended particulate matter. Cont Shelf Res 19:1199–1220
Chardy P, Chevillon C, Clavier J (1988) Major benthic communities of the south-west lagoon of New-Caledonia. Coral Reefs 7:69–75
Clavier J, Chardy P, Chevillon C (1995) Sedimentation of particulate matter in the South-West lagoon of New Caledonia: spatial and temporal patterns. Est Coat Shelf Sci 40:281–294
Dade B, Nowell ARM, Jumars PA (1992) Predicting erosion resistance of muds. Mar Geol 105:285–297
Debenay JP (1987) Sedimentology in the South-West Lagoon of New-Caledonia, SW Pacific. J Coastal Res 3:77–91
Dekker AG, Vos RJ, Peters SWM (2002) Analytical algorithms for lake water TSM estimation for retrospective analyses of TM and SPOT sensor data. Int J Remote Sens 23:15–35
Done T (1982) Patterns in the distribution of coral communities across the central Great Barrier Reef. Coral Reefs 1:95–107
Douillet P (1998) Tidal dynamics of the south-west lagoon of New Caledonia: observations and 2D numerical modelling. Oceanol Acta 21:69–79
Douillet P, Ouillon S, Cordier E (2001) A numerical model for fine suspended sediment transport in the south-west lagoon of New-Caledonia. Coral Reefs 20:361–372
Doxaran D, Froidefond JM, Lavender S, Castaing P (2002) Spectral signature of highly turbid waters, Application with SPOT data to quantify suspended particulate matter concentrations. Rem Sens Env 81:149–161
Durand N, Fiandrino A, Fraunie P, Ouillon S, Forget P, Naudin JJ (2002) Suspended matter dispersion in the Ebro ROFI: an integrated approach. Cont Shelf Res 22:267–284
Estournel C, Kondrachoff V, Marsaleix P, Vehil R (1997) The plume of the Rhone: numerical simulation and remote sensing. Cont Shelf Res 17:899–924
Fargion GS, Mueller JL (2000) Ocean Optics for satellite ocean color sensor validation, rev. 2. NASA Technical Memorandum 209966, Goddard Space Flight Center, Greenbelt MD
Forget P, Ouillon S (1998) Surface suspended matter off the Rhône river mouth from visible satellite imagery. Oceanol Acta 21:739–749
Hallermeier RJ (1981) Terminal settling velocity of commonly occurring sand grains. Sedimentology 28:859–865
Hu C, Carder KL, Müller-Karger FE (2000) Atmospheric correction of SeaWIFS imagery over turbid coastal waters; a practical method. Remote Sens Environ 74:195–206
Hu C, Müller-Karger FE, Andréfouët S, Carder KL (2001) Atmospheric correction and cross-calibration of LANDSAT-7/ETM+ imagery over aquatic environments: A multiplatform approach using SeaWiFS/MODIS. Remote Sens Environ 78:99–207
Hudson JH (1981) Growth rates in *Montastraea annularis*: a record of environmental change in Key Largo Coral Reef Marine Sanctuary, Florida. Bull Mar Sci 31:444–459
Jarrige F, Radok R, Krause G, Rual P (1975) Courants dans le lagon de Nouméa (Nouvelle Calédonie). Déc.74-janv. 75. Rapp ORSTOM (Nouméa) and H Lamb Inst Oceanogr, Flinders Univ S Australia, 6 pp
Jin JY, Lee DY, Park JS, Park KS, Yum KD (2001) Monitoring of suspended sediment concentration using vessels and remote sensing. In: McAnally WH, Mehta AJ (eds) Coastal and estuarine fine sediment processes. Elsevier, Amsterdam, pp 287–299
Jorgensen PV, Edelvang K (2000) CASI data utilized for mapping suspended matter concentrations in sediment plumes and verification of 2D hydrodynamic modelling. Int J Remote Sens 21:2247–2258
Keiner LE, Yan XH (1998) A neural network model for estimating sea surface chlorophyll and sediments from Thematic Mapper imagery. Remote Sens Environ 66:153–165
Khorram S, Cheshire H, Geraci AL, La Rosa G (1991) Water quality mapping of Augusta Bay, Italy from Landsat-TM data. Int J Remote Sens 12:803–808
Kleypas JA, McManus JW, Menez LAB (1999) Environmental limits to coral reef development: where do we draw the line? Am Zool 39:146–159
Krone RB (1962) Flume studies of the transport of sediment in estuarial shoaling processes. Tech Rep, Hydraulic Eng Lab and Sanitary Eng Res Lab, Univ California, Berkeley, CA
Larcombe P, Woolfe KJ (1999) Increased sediment supply to the Great Barrier Reef will not increase sediment accumulation at most coral reefs. Coral Reefs 18:163–169
Larcombe P, Ridd PV, Prytz A, Wilson B (1995) Factors controlling suspended sediment on inner-shelf coral reefs, Townsville, Australia. Coral Reefs 14:163–171
Lazure P, Salomon JC (1991) Coupled 2-D and 3-D modelling of coastal hydrodynamics. Oceanol Acta 14:173–180
Lee Z, Carder KL, Chen RF, Peacock TG (2001) Properties of the water column and bottom derived from Airborne Visible Infrared Imaging Spectrometer (AVIRIS) data. J Geophys Res 106:11639–11651
Mikkelsen OA (2002) Variation in the projected surface area of suspended particles: implications for remote sensing assessment of TSM. Remote Sens Environ 79:23–29
Mobley CD (1999) Estimation of the remote-sensing reflectance from above-surface measurements. Appl Opt 38:7442–7455
Morlière A, Crémoux JL (1981) Observations de courant dans le lagon, de Février à Août 1981. Rap Sci Tech ORSTOM, p 50
Mueller JL, Davis C, Arnone R, Frouin R, Carder K, Lee ZP, Steward RG, Hooker S, Mobley CD, McLean S (2000) Above-water radiance and remote sensing reflectance measurement and analysis protocols. In: Fargion GS, Mueller JL (eds) Ocean optics for satellite ocean color sensor validation, rev. 2. NASA, Goddard Space Flight Center, Greenbelt MD, pp 98–107
O'Callaghan J (1999) The oceanography an sedimentology of a coastal embayment: Dumbea Bay, Noumea, New Caledonia. Thesis for the degree of Bachelor of Science in Earth Sciences, School of Earth Sciences, James Cook Univ, S Australia, p 86
Ouillon S (2003) An inversion method for reflectance in stratified turbid waters. Int J Remote Sens 24:335–358
Ouillon S, Caussade B (1991) Numerical simulation and remote sensing, two techniques applied on the Gambia estuary. In: Ben Sari D, Brebbia CA, Ouazar D (eds) Computer methods in water resources 2, vol 3. Springer, Berlin Heidelberg New York, pp 209–220
Partheniades E (1965) Erosion and deposition of cohesive soils. J Hydraul Div 91:105–139
Puls W, Doerffer R, Sündermann J (1994) Numerical simulation and satellite observations of suspended matter in the North Sea. IEEE J Ocean Eng 19:3–9
Ritchie JC, Cooper CM, Schiebe FR (1990) The relationships of MSS and TM digital data with suspended sediments, chlorophyll and temperature in Moon Lake, Mississippi. Remote Sens Environ 33:137–148
Schaaff E, Grenz C, Pinazo C (2002) Erosion of particulate inorganic and organic matter in the Gulf of Lion. C R Geosci 334:1071–1077
Schiller H, Doerffer R (1999) Neural network for emulation of an inverse model—operational derivation of Case II water properties from MERIS data. Int J Remote Sens 20:1735–1746
Soulsby RL (1997) Dynamics of marine sands. Thomas Telford, London
Sydor M (1980) Remote sensing of particulate concentrations in water. Appl Opt 19:2794–2800

Tassan S (1987) Evaluation of the potential of the Thematic Mapper for marine application. Int J Remote Sens 8:1455–1478
Thomsen LA, Gust G (2000) Sediment erosion thresholds and characteristics of resuspended aggregates on the western European continental margin. Deep-Sea Res I 47:1881–1897
Topliss BJ, Amos CL, Hill PR (1990) Algorithms for remote sensing of high concentration, inorganic suspended sediment. Int J Remote Sens 11:947–966
Wass PD, Marks SD, Finch JW, Leeks GJL, Ingram JK (1997) Monitoring and preliminary interpretation of in-river turbidity and remote sensing imagery for suspended sediment transport studies in the Humber catchment. Sci Tot Environ 194/195:263–283
Woolfe KJ, Larcombe P (1999) Terrigenous sedimentation and coral reef growth: a conceptual framework. Mar Geol 155:331–345
You Y, Hou M (1992) Remote Sensing analysis of the suspended sediment transport in Lingdingyang. China Ocean Eng 6:331–349